Yogita Kalra

final thesis (DEEPAK)

PHD

Document Details

Submission ID
trn:oid:::27535:140637320

Submission Date
May 27, 2026, 2:15 PM GMT+5:30

Download Date
May 27, 2026, 2:17 PM GMT+5:30

File Name
final thesis (DEEPAK).pdf

File Size
1.1 MB

23 Pages

5,647 Words

33,952 Characters

5% Overall Similarity

The combined total of all matches, including overlapping sources, for each database.

Filtered from the Report

- Bibliography
- Small Matches (less than 10 words)

Match Groups

21 Not Cited or Quoted 5%
Matches with neither in-text citation nor quotation marks

0 Missing Quotations 0%
Matches that are still very similar to source material

0 Missing Citation 0%
Matches that have quotation marks, but no in-text citation

0 Cited and Quoted 0%
Matches with in-text citation present, but no quotation marks

Top Sources

3% Internet sources
3% Publications
3% Submitted works (Student Papers)

Integrity Flags

0 Integrity Flags for Review

Our system's algorithms look deeply at a document for any inconsistencies that would set it apart from a normal submission. If we notice something strange, we flag it for you to review.

A Flag is not necessarily an indicator of a problem. However, we'd recommend you focus your attention there for further review.

Match Groups

- **21** Not Cited or Quoted 5%
  Matches with neither in-text citation nor quotation marks
- **0** Missing Quotations 0%
  Matches that are still very similar to source material
- **0** Missing Citation 0%
  Matches that have quotation marks, but no in-text citation
- **0** Cited and Quoted 0%
  Matches with in-text citation present, but no quotation marks

Top Sources

- 3% Internet sources
- 3% Publications
- 3% Submitted works (Student Papers)

Top Sources

The sources with the highest number of matches within the submission. Overlapping sources will not be displayed.

1	Publication	Deepika Tyagi, Abida Parveen, Vijay Laxmi, Ahsan Irshad et al. "THz beat note gen...	<1%
2	Publication	M. Amraie, T. Fathollahi-Khalkhali, A. Aghamohammadi, E. Lotfi. "Coupling Perfor...	<1%
3	Publication	R. Flores-Cruz, L.A. Bautista-Aguilar, J.F. Acosta-Palacios, M. Arteaga-Varela et al. "...	<1%
4	Internet	www.scribd.com	<1%
5	Student papers	University of Glasgow on 2025-08-14	<1%
6	Student papers	University of Sheffield on 2024-09-06	<1%
7	Internet	etheses.whiterose.ac.uk	<1%
8	Publication	Anders Bjarklev, Jes Broeng, Araceli Sanchez Bjarklev. "Photonic Crystal Fibres", S...	<1%
9	Student papers	JIS University on 2024-12-30	<1%
10	Publication	Petr Brázda, Pingo Mutombo, Martin Ondráček, Cinthia Antunes Corrêa, Jaromír ...	<1%

11 Student papers

University of Surrey on 2015-02-25 <1%

12 Internet

apps.dtic.mil <1%

13 Student papers

Malaviya National Institute of Technology on 2011-06-11 <1%

14 Student papers

University of Sydney on 2023-08-14 <1%

15 Publication

Zhipeng Qi, Guohua Hu, Xiumin Song, Hao Sun et al. "Ultracompact topological w... <1%

16 Internet

nlist.inflibnet.ac.in <1%

17 Internet

ris.utwente.nl <1%

18 Internet

tdr.lib.ntu.edu.tw <1%

19 Internet

wiredspace.wits.ac.za <1%

ABSTRACT

Periodic dielectric structures offer a powerful means of controlling light at the wavelength scale. In this study, the propagation of single photon wave packets is investigated in a two dimensional hexagonal photonic crystal composed of gallium arsenide (GaAs) rods in air, operating in the near infrared region. By examining the photonic band structure as a function of the normalized rod radius r/a, a complete transverse magnetic (TM) photonic bandgap is identified near $r/a = 0.274$. A lattice constant of $a = 422$ nm is selected so that the operating wavelength of 810 nm lies well within this bandgap region. A W1 photonic crystal waveguide is formed by removing a single row of rods from the periodic lattice. The defect channel allows guided modes to propagate within the photonic bandgap region. Finite difference time domain (FDTD) simulations were used to examine the propagation of a Gaussian wave packet through the waveguide. The transmission coefficient was calculated to be approximately $T \approx 0.983$, corresponding to an insertion loss of about0.073 dB. The simulated field profiles indicate that most of the electromagnetic energy remains confined inside the defect channel during propagation, while only small losses occur near the input and output sections. Overall, the study shows that a standard GaAs W1 photonic crystal waveguide can support efficient single-photon transport in the near infrared region. This type of structure could be useful for low loss integrated quantum photonic devices.

Keywords: photonic crystal waveguide, W1 waveguide, GaAs, photonic bandgap, single-photon transport, FDTD simulation, quantum photonics, near-infrared photonics.

CHAPTER 1

INTRODUCTION

This chapter describes the scientific basis for the study of single photon propagation in photonic crystal waveguides. Included are an overview of integrated quantum photonics, a discussion of the importance of low loss optical channels, a review of previous research, an identification of the present research gap, a description of the objectives and extent of the current study, and a synopsis of the structure of the thesis.

1.1 Background

Quantum information has emerged as one of most influential areas of modern physics, significantly reshaping existing concepts of computation and communication in recent times. By utilizing uniquely quantum mechanical effects, particularly superposition and entanglement, Researchers have come up with communication results capable of achieving security levels with the help of quantum mechanical effects, particularly superposition and entanglement, unattainable within classical frameworks. At the same time, quantum computing systems perform certain computational tasks much more efficiently than traditional algorithms [1]. Photons are especially attractive for carrying quantum information as compared to other platforms used for these technologies. They interact weakly with the surrounding medium which minimizes environmental decoherence during propagation. Information can be coded using photons through various degrees of freedom such as polarization, spatial modes, time bins and frequency states. Apart from this, photons enable ultrafast information transfer as they propagate at the speed of light [2].

In quantum photonic technologies, photons should be transmitted, controlled, and measured with minimal loss when implemented. Signal degradation occurs during propagation in conventional fibre optic communication networks. Optical amplification at intermediate repeater stations are responsible for compensating it. Quantum communication systems, however, cannot rely on the same strategy. The no-cloning theorem prohibits exact duplication of an arbitrary unknown quantum state. It preventing direct amplification of quantum signals without disturbing the encoded information [3]. Consequently, photon loss during transmission represents a fundamental challenge for quantum photonic platforms. This limitation demands

the development of waveguiding structures with exceptionally low propagation loss to ensure reliable transport of quantum optical signals.

Compact and scalable optical systems can now be realized with the help of integrated photonics. Integrated photonic platforms implement optical functions directly on planar chips, as opposed to building optical circuits from discrete free space components. Circuits are made up of microfabricated components such waveguides, beam splitters, resonators, and photodetectors. Large scale photonic integration is supported by such architectures, which offer enhanced phase stability, a smaller device footprint, and compatibility with current, well established semiconductor fabrication technologies [3].

Among the various III–V semiconductor materials investigated for integrated quantum photonics, gallium arsenide (GaAs) has attracted considerable attention. It is advantageous for electrical and optical characteristics in the near infrared spectrum. Strong optical field confinement within subwavelength structures is made possible by GaAs's comparatively high refractive index (about 3.6 in the near infrared). For integrated waveguiding applications, it is advantageous [6], [11]. Furthermore, its direct bandgap enables effective communication between embedded quantum emitters, especially self assembled InGaAs quantum dots, and confined optical modes [9], [11], and [12]. The material platform is particularly well suited for the fabrication of on chip single photon sources coupled to guided photonic modes because the emission wavelengths of these quantum dots naturally lie within the working spectral range of GaAs-based photonic devices [9], [11], and [12].

1.2 Problem Statement

Despite many advancements in integrated quantum photonic technologies, the effective transmission of single photons across wavelength scale waveguide structure remains an issue that needs to be addressed. Traditional ridge waveguides provide effective optical confinement, which operate on the basis of total internal reflection. Their capacity to regulate group velocity and modal dispersion is still restricted, though. On the other hand, bandgap assisted light confinement is supported by photonic crystal waveguides, which are produced by introducing line defects within periodic dielectric lattices. Additionally, it improved dispersion

engineering's versatility [7], [8]. Because of these characteristics, they are useful for integrated quantum photonic applications. There are lots of issues like coupling losses, manufacturing flaws, and pulse distortion within dispersive guiding regimes that continue to limit practical application.

Despite a great deal of research on photonic crystal waveguides, the propagation behaviour of individual photon wave packets in a typical W1 GaAs rod type hexagonal lattice structure operating close to the 810 nm spectral region under ideal geometric conditions has not been thoroughly investigated. The main goal of the current effort is to address this problem.

1.3 Motivation

The work is motivated by ongoing developments in integrated quantum photonics and semiconductor single photon technologies. Many people believe that quantum dots operating in the 800 to 930 nm wavelength range are effective on demand single photon emitters appropriate for quantum optical applications [11]. These emitters need to be integrated with waveguiding platforms that can allow low loss photon transmission on a chip in order to create scalable photonic quantum circuits. Because of their periodic dielectric geometry, which allows for both flexible dispersion engineering and robust optical confinement, photonic crystal waveguides are a great option. Furthermore, earlier research has shown that single photon propagation in linear dielectric media accurately described by classical electromagnetic theory [21]. Therefore, a good framework for examining the dynamics of single photon wave packets in such systems is provided by finite difference time domain (FDTD) simulation.

1.4 Literature Review

Eli Yablonovitch and Sajeev John independently established the conceptual underpinnings of photonic crystals in 1987. Yablonovitch suggested that by creating photonic bandgaps, periodically structured dielectric media may prevent spontaneous emission [4]. In disordered dielectric superlattices, John showed that photon localisation is possible [5]. Later, John D. Joannopoulos and colleagues devised a thorough electromagnetic treatment of photonic crystals [6]. They demonstrated that dielectric rod type setups can sustain relatively broad TM polarised photonic bandgaps by formulating Maxwell's equations in periodic dielectric systems as an eigenvalue issue.

16

Subsequent studies focused extensively on dispersion engineering and slow light phenomena in photonic crystal waveguides. Thomas F. Krauss investigated the slow light regime near photonic band edges and demonstrated that strong reductions in group velocity can substantially enhance light matter interaction [7]. In related work, Masaya Notomi reviewed several unconventional optical phenomena associated with strongly modulated photonic crystals, including anomalous dispersion and negative refraction near Brillouin-zone boundaries [8].

Further evidence that photonic crystal platforms are viable options for integrated quantum photonics has come from experimental developments. Near unity coupling efficiencies between semiconductor quantum dots and photonic crystal waveguide modes in GaAs membrane devices were reported by Michele Arcari and colleagues [9]. Later, Alec Goban and associates showed that atoms placed close to photonic crystal waveguides might produce enhanced super radiant emission [10]. The expanding significance of integrated quantum photonic frameworks was highlighted in a thorough analysis by Peter Lodahl, Sahin Mahmoodian, and Søren Stobbe that summarised significant advancements in connecting single photons and quantum emitters with photonic nanostructures [11].

Lund-Hansen and co-workers [12] demonstrated efficient broadband coupling of quantum dots to photonic crystal waveguides through band edge effects. These contributions collectively established GaAs photonic crystal waveguides as one of the most advanced platforms for quantum optical experiments.

More recent work has explored topological protection as a route to robust photon transport. Barik and collaborators [13] demonstrated a topological quantum optics interface using helical photonic crystal waveguides. Ozawa and co-workers [14] reviewed topological photonics broadly, covering topological invariants and their implications for robust guided transport. Kuruma and colleagues [23] demonstrated experimentally that topological slow-light photonic crystal waveguides in GaAs could support Purcell enhanced single photon emission with group indices exceeding 20 and robust propagation through sharp bends. Smirnova and co authors [15] explored nonlinear topological photonic effects.

The theoretical basis for using classical FDTD as a quantum photonic modelling tool was established by Smith and Raymer [16], who developed a rigorous photon wave function

framework demonstrating that the classical field envelope and the single photon probability amplitude obey identical equations in linear dielectric media. Hawton [21] explicitly validated this correspondence for pulse propagation problems, providing the key justification for the present numerical approach. The open source MEEP simulation package developed by Ardavan F. Oskooi and collaborators at Massachusetts Institute of Technology provides a versatile finite difference time domain (FDTD) framework widely used for the analysis of photonic crystal structures. The software supports several features essential for photonic simulations, including Bloch periodic boundary conditions, mode source excitation, and electromagnetic power flux calculations [18].

1.5 Research Gap

Photonic crystal waveguides have been studied extensively for integrated and quantum photonic applications, with most reported work concentrating on TE-polarized slab structures based on triangular air-hole lattices in silicon or GaAs membranes. By comparison, TM-polarized transport in rod-type hexagonal GaAs photonic crystals has received relatively limited attention, especially in the near-infrared region around 810 nm that is relevant for quantum-dot-based single-photon devices.

In addition, much of the existing literature has focused on photonic band engineering, slow-light effects, or light–matter interaction in emitter-coupled systems. Fewer studies have examined how localized single-photon wave packets propagate through a conventional W1 photonic crystal waveguide, particularly in terms of field confinement, pulse evolution, and transmission behaviour under optimized bandgap conditions. A clear connection between bandgap optimization, operating wavelength selection, and low-loss photon transport in TM-polarized hexagonal rod-type GaAs structures has therefore remained insufficiently explored using combined band-structure and FDTD analysis. The present work is intended to address this area.

1.6 Objectives

The principal objectives of this thesis are:

(i) To calculate the TM photonic band structure of a hexagonal GaAs rod lattice and identify the complete bandgap as a function of r/a.

(ii) To optimize r/a for maximum bandgap width and select a lattice constant placing 810 nm within the bandgap.

(iii) To design a W1 waveguide by introducing a line defect into the optimized lattice.

(iv) To simulate Gaussian wave packet propagation through the W1 waveguide using FDTD and analyse the resulting field distributions.

(v) To quantify the transmission coefficient and interpret it as the single-photon transport probability.

(vi) To discuss the results in context of existing literature.

1.7 Scope of Work

The scope is limited to two dimensional TM polarization electromagnetic analysis of a GaAs rod type hexagonal photonic crystal W1 waveguide. Three dimensional slab effects, material dispersion, absorption losses, and fabrication imperfections are outside the scope of this study. The results represent the idealized propagation regime and should be interpreted accordingly when comparing to practical fabricated devices.

1.8 Organization of the Thesis

Chapter 1 has provided the background, motivation, literature review, research gap, objectives, and scope. Chapter 2 describes the photonic crystal design, theoretical framework, numerical methodology, results, and discussion. Chapter 3 summarizes the findings, states contributions, discusses limitations, and outlines future research directions. A complete IEEE formatted reference list follows Chapter 3.

CHAPTER 2

RESEARCH WORK AND PROPOSED METHODOLOGY

This chapter presents the photonic crystal design, the theoretical framework, the numerical methodology, and the results obtained from band-structure calculations and time-domain simulations. The chapter follows the logical progression from structural design through physical modelling to simulation and result analysis.

2.1 Lattice Geometry and Photonic Crystal Design

The photonic crystal investigated in this work consists of a two-dimensional hexagonal lattice of cylindrical GaAs rods embedded in air. The structure is fully characterized by the lattice constant "a" the centre to centre spacing between adjacent rods and the rod radius "r". GaAs possesses a refractive index of approximately 3.6 in the near infrared, yielding a dielectric constant of approximately 13. This high refractive index contrast between GaAs and air is a key enabling factor for the formation of wide photonic bandgaps, since the contrast determines the size of the frequency gap that opens at Brillouin zone boundaries [6]. The hexagonal lattice provides a more circular Brillouin zone than the square lattice, which promotes isotropic bandgap formation in all in plane directions. Here, Figure 1 shows the geometry lattice.

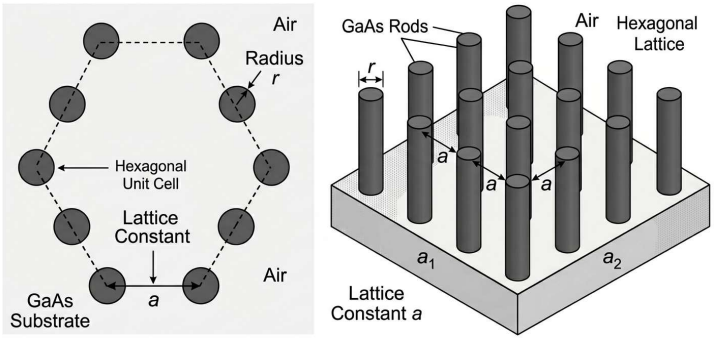

Figure 1. Schematic of a hexagonal lattice of GaAs rods in air. The lattice constant *a* defines the spacing between neighbouring rods, whereas *r* denotes the rod radius. The periodic dielectric arrangement supports photonic bandgap formation and optical confinement.

2.2 Electromagnetic Eigenvalue Formulation

Electromagnetic propagation within the periodic dielectric structure is governed by Maxwell's equations. In the frequency domain representation, the magnetic field $H(r)$ can be expressed through the following eigenvalue equation:

$$\nabla \times \left(\frac{1}{\varepsilon(r)} \nabla \times H(r) \right) = \left(\frac{\omega}{c} \right)^2 H(r) \quad (1)$$

Here, $\varepsilon(r)$ denotes the position dependent dielectric permittivity, ω represents the angular frequency, and c corresponds to the speed of light in vacuum. Due to the periodic nature of the dielectric lattice, the electromagnetic eigenmodes satisfy Bloch's theorem and may therefore be expressed in the following form:

$$H_{nk}(r) = e^{ik \cdot r} u_{nk}(r) \quad (2)$$

where $u_{(nk)}(r)$ represents the lattice-periodic component of the Bloch mode, n denotes the band index, and k corresponds to the Bloch wave vector[6].Solving this eigenvalue problem across the irreducible Brillouin zone yields the photonic band structure $\omega_n(k)$, which identifies allowed and forbidden optical frequency ranges. For rod-type geometries, TM modes (with E field parallel to the rod axis) exhibit pronounced bandgaps because the high dielectric rods act as effective resonators for the longitudinal electric field component. All calculations and simulations in this work are therefore performed for TM polarization.

Optical frequencies are represented using the dimensionless normalized frequency

$$\frac{a}{\lambda} = \frac{\omega a}{2\pi c},$$

which renders the analysis scale independent. The photonic band structure is calculated along the high-symmetry path $\Gamma \rightarrow K \rightarrow M \rightarrow \Gamma$ of the hexagonal Brillouin zone. The resulting dispersion diagram, shown in Figure 2, reveals a complete TM photonic bandgap a frequency interval in which no propagating TM mode exists for any in plane wave vector.

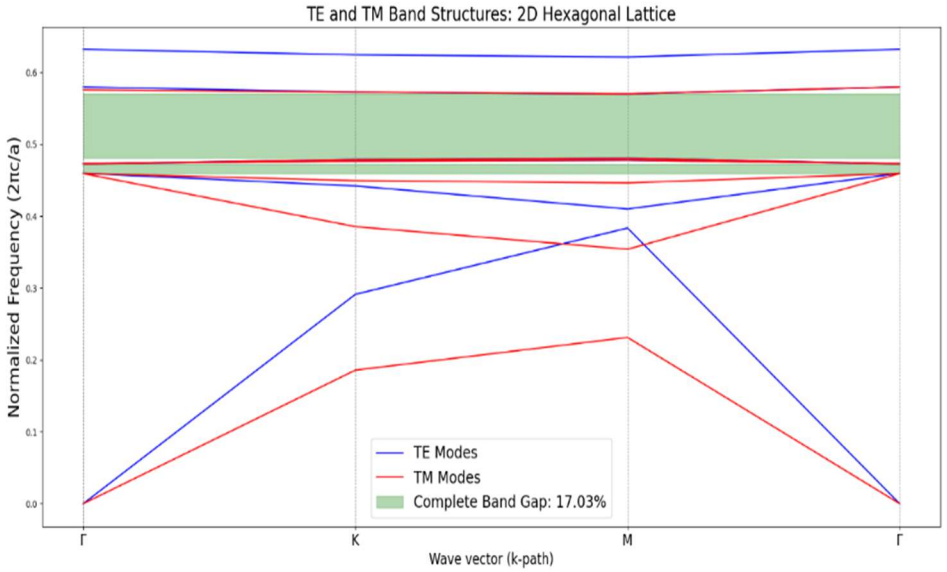

Figure 2. Photonic band structure of the hexagonal lattice calculated along the high-symmetry directions of the irreducible Brillouin zone. The shaded region indicates the complete TM photonic bandgap where propagation through the bulk crystal is prohibited.

2.3 Bandgap Optimization

To optimize the confinement properties of the structure, the TM bandgap width is investigated as a function of the normalized rod radius r/a. A systematic sweep reveals that the bandgap width reaches its maximum near r/a = 0.274. For values below this range, the dielectric filling fraction becomes too small to sustain strong Bragg scattering throughout the Brillouin zone. Conversely, at larger r/a values, neighbouring rods become increasingly close, causing the structure to behave more like an effective homogeneous medium. That weaken the refractive index contrast responsible for photonic bandgap formation. The dependence of the bandgap width on the r/a ratio is illustrated in Figure 3.

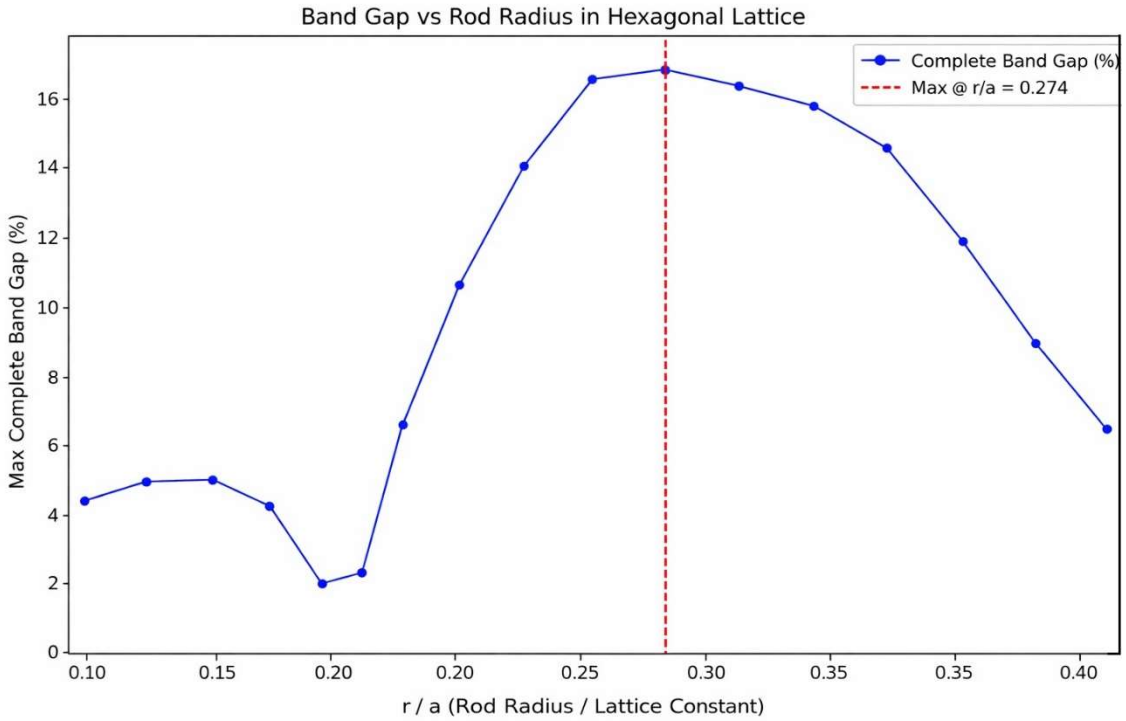

Figure 3. Dependence of the photonic bandgap width on the normalized rod-radius ratio r/a. The maximum bandgap is obtained near $\mathrm{r/a} = 0.274$, which corresponds to the optimized structural configuration employed in the waveguide simulations.

After choosing $r/a = 0.274$ as the optimized structural ratio, the lattice constant was fixed at $a = 422nm$ such that the operating wavelength of $810\ nm$ remained within the central region of the primary TM photonic bandgap. Positioning the operating wavelength away from the band-edge regions helps reduce the effects of group velocity dispersion as well as disorder induced scattering. The calculated TM band structure shown in Figure 4, expressed in normalized wavelength units, verifies that the wavelength of 810 nm lies inside the primary bandgap along all major high symmetry directions of the Brillouin zone.

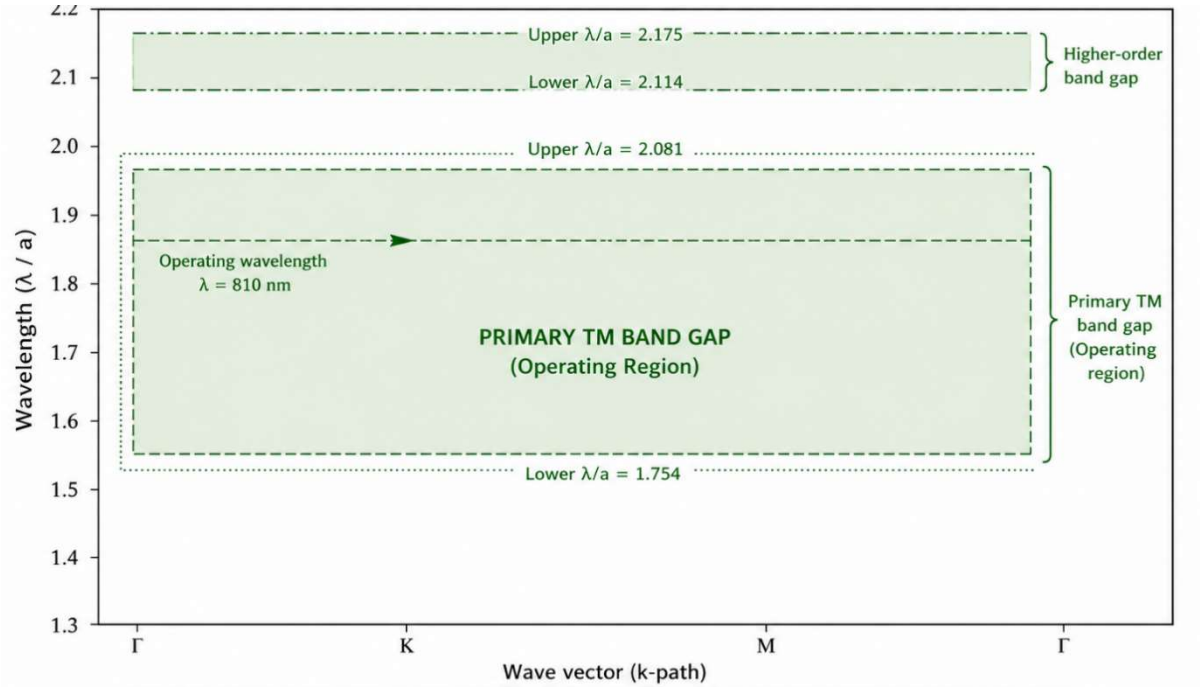

Figure 4. Complete TM photonic bandgap regions represented in normalized wavelength units along the Γ-K-M-Γ symmetry directions of the hexagonal Brillouin zone. The shaded regions indicate wavelength intervals where electromagnetic propagation through the bulk photonic crystal is forbidden. The chosen wavelength satisfies the bandgap condition for guided propagation.

2.4 Waveguide Formation and Single-Photon Representation

2.4.1 W1 Waveguide Design

A photonic crystal waveguide is created by introducing a controlled line defect into the periodic lattice through the removal of a single row of GaAs rods. This standard W1 configuration creates a channel region bordered on both sides by the intact photonic crystal. The guiding mechanism is the photonic bandgap of the surrounding crystal: frequencies within the bandgap cannot propagate in the bulk crystal on either side of the defect, so electromagnetic energy at those frequencies has no escape route and remains localized within the defect channel [7], [8]. This bandgap guided confinement is fundamentally different from total internal reflection guiding and is in principle lossless in a perfect two dimensional crystal. The W1 waveguide structure is illustrated in Figure 5.

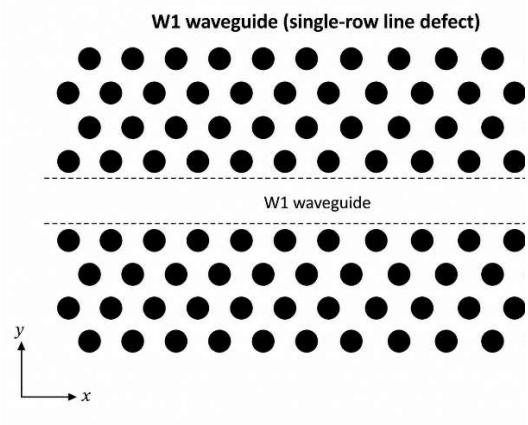

Figure 5. W1 photonic crystal waveguide formed by removing a single row of dielectric rods from the hexagonal lattice. The defect channel supports guided modes within the photonic bandgap and enables confined optical propagation.

2.4.2 Classical Representation of Single Photon Wave Packets

In linear dielectric media, Maxwell's equations are amplitude independent, the propagation dynamics of an electromagnetic wave packet depend only on the geometry and dielectric properties of the medium, not on the field amplitude. Consequently, a single photon wave packet and a classical wave packet with the same spatial and temporal envelope obey identical equations of motion and evolve identically [16], [21]. The probability amplitude for finding the photon at a given position equals the classical field amplitude, and the classical power transmission coefficient T equals the single-photon transport probability. FDTD simulation can therefore be used directly to compute single photon transmission probabilities.

The single photon wave packet is represented by a Gaussian modulated carrier pulse:

$$E(t) = E_0 \exp\left[-\frac{(t-t_0)^2}{2\sigma^2}\right] e^{-i\omega_0 t}$$

where E_0 is the field amplitude, t_0 is the pulse centre, σ is the temporal width, and $\omega_0 = 2\pi c/810$ nm is the carrier frequency. The Gaussian envelope minimizes the time-bandwidth product and ensures a spectrally narrow pulse whose entire bandwidth lies within the photonic bandgap.

2.5 Numerical Methodology

The FDTD simulations were carried out using the MEEP package [18], an open-source electromagnetic simulation software developed at MIT for photonic and nanophotonic modelling. MEEP solves Maxwell's curl equations on a staggered Yee grid using a time domain finite difference scheme [17]. The computational domain consists of the hexagonal GaAs photonic crystal containing the W1 defect waveguide. Perfectly matched layer (PML) boundary conditions were applied at the outer edges of the simulation region to suppress artificial reflections from the boundaries. A sufficiently fine spatial discretization was used to accurately represent the GaAs air interfaces, and numerical convergence was confirmed by comparing results across different grid resolutions.

A Gaussian-modulated TM polarized source is placed at the waveguide input, centred at 810 nm. Power flux monitors at the input and output planes record the electromagnetic power throughout the simulation. The transmission coefficient and insertion loss were calculated as:

$$T = \frac{P_{out}}{P_{in}}$$

$$\text{Loss}(dB) = -10\log_{10}(T)$$

In the linear optical regime, the calculated transmission coefficient also represents the probability of single-photon transport through the waveguide [21].

2.6 Results and Analysis

2.6.1 Field Confinement and Pulse Propagation

The injected Gaussian wave packet propagates along the W1 defect waveguide with high lateral confinement and excellent transmission, according to time domain simulations. Because the working frequency is within the major TM photonic bandgap, radiation leakage into the surrounding photonic crystal region is still strongly inhibited. There are no propagating bulk modes. Figure 6 shows the electric field distribution's temporal change during transmission.

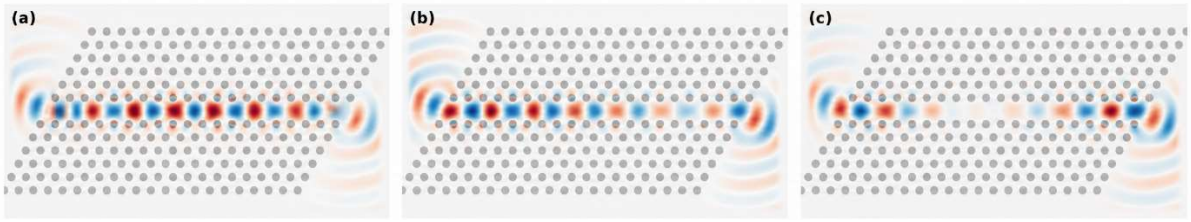

Figure 6: Temporal evolution of the electric field profile during Gaussian pulse transmission in the W1 photonic crystal waveguide: (a) pulse injection into the defect channel, (b) field propagation through the central guiding region, and (c) pulse transmission near the waveguide output. The electromagnetic field remains strongly confined within the defect channel throughout propagation, demonstrating efficient waveguiding and suppression of lateral radiation leakage by the surrounding photonic crystal lattice.

The field snapshots confirm that the guided mode propagates predominantly along the defect channel without significant scattering or diffraction. A slight spatial broadening of the pulse envelope is observable over the course of propagation, consistent with normal group velocity dispersion of the guided mode different spectral components of the pulse travel at slightly different group velocities. The magnitude of this broadening is modest, confirming that the operating point is not in the strongly dispersive near band edge region. Small residual leakage near the waveguide terminations is attributable to coupling losses at the excitation and output regions rather than to lateral radiation during propagation.

2.6.2 Transmission Characteristics

The transmission characteristics are evaluated from the normalized power flux at the input and output monitor planes. The computed power values are:

Table 4.1 Transmission characteristics of the photonic crystal waveguide obtained from FDTD simulations.

Parameter	value
Incident Power, P_{in}	0.0024713
Transmitted Power, P_{out}	0.0024303
Transmission Coefficient, T	0.9834
Insertion Loss	0.073 dB
Transmission Efficiency	98.34%

In the quantum optical interpretation established by the classical quantum correspondence [16], [21], T = 0.983 simultaneously represents the classical power transmission and the probability

of single photon transport through the waveguide. These results suggest highly efficient guided mode propagation within the idealized waveguide structure. The small residual loss (~1.7%) primarily originates from coupling inefficiencies near the source and output interfaces, finite size effects associated with the simulated photonic crystal region. The weak evanescent leakage through the limited number of crystal periods surrounding the defect channel, rather than from material absorption or fabrication induced disorder.

2.7 Comparison with Existing Photonic Crystal Studies

The calculated transmission coefficient of $T \approx 0.983$ is consistent with values reported in previous studies of photonic crystal waveguides. Experimental investigations on GaAs based W1 structures have demonstrated quantum dot coupling efficiencies approaching 98.4% under optimized conditions [9]. Although coupling efficiency and end to end transmission correspond to different physical processes, the transmission obtained in the present simulation remains comparable in magnitude to these experimentally reported values. Earlier numerical studies employing finite difference time domain (FDTD) techniques for idealized two dimensional W1 photonic crystal waveguides have typically reported transmission coefficients within the range from 0.95 to 0.99. The simulated value of 0.983 therefore falls within the expected performance range for standard W1 geometries.

The results also show that selecting an operating wavelength near the centre of the photonic bandgap supports efficient pulse propagation with relatively small distortion. By contrast, wavelengths located closer to the photonic band edges experience stronger slow light effects and increased dispersion, which can adversely influence pulse transmission.

Near band edge operation would yield stronger light matter interaction through the Purcell enhancement but at the cost of increased group velocity dispersion, stronger sensitivity to disorder, and greater pulse broadening. The present operating regime is therefore preferable for applications requiring high fidelity quantum state transmission. The explicit invocation of the Smith -Raymer-Hawton correspondence [16], [21] to recast the FDTD result as a single-photon transport probability provides a direct bridge between classical computational photonics and quantum information science, contributing to the methodological toolkit for quantum photonic device modelling.

It should be noted that the two dimensional numerical model does not capture three dimensional effects present in physical slab structures, including out of plane radiation losses, polarization mixing, and the modified guided-mode dispersion of a finite thickness membrane. Material absorption and fabrication imperfections are also excluded. The insertion loss of 0.073 dB should therefore be regarded as a theoretical lower bound rather than a prediction of performance in fabricated devices.

CHAPTER 3

CONCLUSION AND FUTURE PERSPECTIVE

3.1 Summary of Findings

This thesis has presented a combined band-structure and time domain numerical investigation of single photon wave packet propagation in a two dimensional GaAs hexagonal photonic crystal W1 waveguide. The normalized rod radius r/a was optimized to r/a = 0.274 for maximum TM bandgap width, and a lattice constant a = 422 nm was selected to place the operating wavelength of 810 nm within the primary TM bandgap. A standard W1 waveguide was formed by removing a single row of rods from the periodic lattice. FDTD simulations using MEEP demonstrated strong transverse confinement of a Gaussian wave packet during propagation, yielding a transmission coefficient T ≈ 0.9834 and an insertion loss of approximately 0.073 dB. Under the classical-quantum correspondence for single-photon wave packets in linear media [16], [21], this transmission coefficient simultaneously represents the classical power transmission and the quantum mechanical probability of single-photon transport through the waveguide.

3.2 Main Contributions

The contributions of this thesis are as follows. First, the study provides a systematic demonstration of the connection between bandgap optimization (via the r/a sweep) and achieved transmission efficiency in a GaAs rod type hexagonal photonic crystal W1 waveguide, which had not been explicitly established for this specific geometry and wavelength through combined band structure and FDTD analysis. Second, the work explicitly applies the Smith-Raymer-Hawton classical quantum correspondence to interpret FDTD simulation results in a quantum optical framework, contributing to the methodological toolkit for quantum photonic device analysis. Third, the study characterizes the complete TM bandgap map in normalized wavelength units for the optimized geometry, providing a direct design guide for selecting operating wavelengths for single photon sources with finite spectral linewidths.

3.3 Limitations

The present study is subject to several limitations. The two-dimensional model does not capture out of plane radiation losses that arise in physical slab structures. Material absorption in GaAs and the wavelength dependence of the refractive index have been neglected. The simulations assume a perfectly periodic crystal with no fabrication disorder. The insertion loss of 0.073 dB should be regarded as a theoretical lower bound rather than a prediction of experimentally achievable performance. The study also considers only a single operating wavelength and a single waveguide configuration, and coupling efficiency between external interfaces and the photonic crystal waveguide is outside the scope.

3.4 Practical Implications

The result that a standard W1 geometry can achieve $T > 0.98$ in a properly optimized GaAs photonic crystal suggests that the basic W1 design is a viable starting point for low loss single-photon routing on a chip. The optimization methodology systematic r/a sweep followed by wavelength matched lattice constant selection is directly applicable to other material systems and operating wavelengths, such as GaN for the visible range or silicon carbide for colour centre emitters. The finding that classical FDTD accurately captures single-photon transport means that the full toolkit of FDTD based design parameter sweeps, sensitivity analysis, inverse design can be applied directly to single photon waveguide design problems.

3.5 Future Research Directions

Several natural extensions of the present work are identified. The most immediate is a three dimensional FDTD simulation of an equivalent GaAs slab photonic crystal, which would quantify the degradation in transmission due to out of plane radiation and provide a more realistic performance estimate. Incorporating fabrication disorder through random perturbations of rod positions and radii would quantify disorder sensitivity and establish fabrication tolerances. Dispersion engineered variants of the W1 waveguide, where boundary rod sizes are modified to produce flat band slow light operation, should be compared against the baseline established here. The integration of topological protection for example through a valley Hall phase transition between two crystal domains would combine the bandgap confinement advantages of the present geometry with robustness against backscattering,

building on the demonstration of topological slow-light sources by Kuruma and colleagues [23]. Finally, experimental realization through electron beam lithography patterning of the hexagonal rod array, integration of InGaAs quantum dot emitters, and photoluminescence characterization would validate the numerical predictions and complete the design fabrication characterization cycle.

REFERENCES

[1] J. L. O'Brien, A. Furusawa, and J. Vučković, "Photonic quantum technologies," Nature Photonics, vol. 3, no. 12, pp. 687–695, 2009. doi: 10.1038/nphoton.2009.229.

[2] A. Politi, M. J. Cryan, J. G. Rarity, S. Yu, and J. L. O'Brien, "Silica-on-silicon waveguide quantum circuits," Science, vol. 320, no. 5876, pp. 646–649, 2008. doi: 10.1126/science.1155441.

[3] J. Wang, F. Sciarrino, A. Laing, and M. G. Thompson, "Integrated photonic quantum technologies," Nature Photonics, vol. 14, no. 5, pp. 273–284, 2020. doi: 10.1038/s41566-019-0532-1.

[4] E. Yablonovitch, "Inhibited spontaneous emission in solid-state physics and electronics," Physical Review Letters, vol. 58, no. 20, pp. 2059–2062, 1987. doi: 10.1103/PhysRevLett.58.2059.

[5] S. John, "Strong localization of photons in certain disordered dielectric superlattices," Physical Review Letters, vol. 58, no. 23, pp. 2486–2489, 1987. doi: 10.1103/PhysRevLett.58.2486.

[6] J. D. Joannopoulos, S. G. Johnson, J. N. Winn, and R. D. Meade, Photonic Crystals: Molding the Flow of Light, 2nd ed. Princeton, NJ: Princeton University Press, 2008.

[7] T. F. Krauss, "Slow light in photonic crystal waveguides," Journal of Physics D: Applied Physics, vol. 40, no. 9, p. S266, 2007. doi: 10.1088/0022-3727/40/9/S07.

[8] M. Notomi, "Manipulating light with strongly modulated photonic crystals," Reports on Progress in Physics, vol. 73, no. 9, p. 096501, 2010. doi: 10.1088/0034-4885/73/9/096501.

[9] M. Arcari et al., "Near-unity coupling efficiency of a quantum emitter to a photonic crystal waveguide," Physical Review Letters, vol. 113, no. 9, p. 093603, 2014. doi: 10.1103/PhysRevLett.113.093603.

[10] A. Goban et al., "Superradiance for atoms trapped along a photonic crystal waveguide," Nature Communications, vol. 6, p. 6808, 2015. doi: 10.1038/ncomms7808.

[11] P. Lodahl, S. Mahmoodian, and S. Stobbe, "Interfacing single photons and single quantum dots with photonic nanostructures," Reviews of Modern Physics, vol. 87, no. 2, pp. 347–400, 2015. doi: 10.1103/RevModPhys.87.347.

[12] T. Lund-Hansen et al., "Experimental realization of highly efficient broadband coupling of single quantum dots to a photonic crystal waveguide," Physical Review Letters, vol. 101, no. 11, p. 113903, 2008. doi: 10.1103/PhysRevLett.101.113903.

[13] S. Barik, A. Karasahin, C. Flower, T. Cai, H. Miyake, W. DeGottardi, M. Hafezi, and E. Waks, "A topological quantum optics interface," Science, vol. 359, no. 6376, pp. 666–668, 2018. doi: 10.1126/science.aaq0327.

[14] T. Ozawa et al., "Topological photonics," Reviews of Modern Physics, vol. 91, no. 1, p. 015006, 2019. doi: 10.1103/RevModPhys.91.015006.

[15] D. Smirnova, D. Leykam, Y. Chong, and Y. Kivshar, "Nonlinear topological photonics," Applied Physics Reviews, vol. 7, no. 2, p. 021306, 2020. doi: 10.1063/1.5142397.

[16] B. J. Smith and M. G. Raymer, "Photon wave functions, wave-packet quantization of light, and coherence theory," New Journal of Physics, vol. 9, no. 11, p. 414, 2007. doi: 10.1088/1367-2630/9/11/414.

[17] A. Taflove and S. C. Hagness, Computational Electrodynamics: The Finite-Difference Time-Domain Method, 3rd ed. Norwood, MA: Artech House, 2005.

[18] A. F. Oskooi, D. Roundy, M. Ibanescu, P. Bermel, J. D. Joannopoulos, and S. G. Johnson, "MEEP: A flexible free-software package for electromagnetic simulations by the FDTD method," Computer Physics Communications, vol. 181, no. 3, pp. 687–702, 2010. doi: 10.1016/j.cpc.2009.11.008.

[19] D. Englund, A. Faraon, B. Zhang, Y. Yamamoto, and J. Vučković, "Generation and transfer of single photons on a photonic crystal chip," Optics Express, vol. 15, no. 9, pp. 5550–5558, 2007. doi: 10.1364/OE.15.005550.

[20] T. Yoshie et al., "Vacuum Rabi splitting with a single quantum dot in a photonic crystal nanocavity," Nature, vol. 432, no. 7014, pp. 200–203, 2004. doi: 10.1038/nature03119.

[21] M. Hawton, "Validation of classical modeling of single-photon pulse propagation," Physical Review A, vol. 107, no. 1, p. 013711, 2023. doi: 10.1103/PhysRevA.107.013711.

[22] A. Peruzzo et al., "Quantum walks of correlated photons," Science, vol. 329, no. 5998, pp. 1500–1503, 2010. doi: 10.1126/science.1193515.

[23] K. Kuruma, H. Yoshimi, Y. Ota, R. Katsumi, M. Kakuda, Y. Arakawa, and S. Iwamoto, "Topologically-protected single-photon sources with topological slow light photonic crystal waveguides," Laser & Photonics Reviews, vol. 16, no. 4, p. 2200077, 2022. doi: 10.1002/lpor.202200077.

[24] N. V. Hauff, H. Le Jeannic, P. Lodahl, S. Hughes, and N. Rotenberg, "Chiral quantum optics in broken-symmetry and topological photonic crystal waveguides," Physical Review Research, vol. 4, no. 2, p. 023082, 2022. doi: 10.1103/PhysRevResearch.4.023082.

[25] F. Ding, "Topological photonics for single-photon sources," Light: Science and Applications, vol. 13, no. 19, 2024. doi: 10.1038/s41377-025-02068-6.

[26] A. Javadi, S. Mahmoodian, I. Söllner, and P. Lodahl, "Numerical modelling of the coupling efficiency of single quantum emitters in photonic-crystal waveguides," Journal of the Optical Society of America B, vol. 35, no. 3, pp. 514–522, 2018. doi: 10.1364/JOSAB.35.000514.

[27] S. Mahmoodian, K. Prindal-Nielsen, I. Söllner, S. Stobbe, and P. Lodahl, "Engineering chiral light-matter interaction in photonic crystal waveguides with slow light," Optical Materials Express, vol. 7, no. 1, pp. 43–54, 2017. doi: 10.1364/OME.7.000043.

[28] L. Lu, J. D. Joannopoulos, and M. Soljačić, "Topological photonics," Nature Photonics, vol. 8, no. 11, pp. 821–829, 2014. doi: 10.1038/nphoton.2014.248.